Research Square

Preprints are preliminary reports that have not undergone peer review.
They should not be considered conclusive, used to inform clinical practice,
or referenced by the media as validated information.

TROP2-Mediated Epithelial Reprogramming Drives Radiotherapy Resistance and Therapeutic Vulnerability in Colorectal Cancer

Ji Zhu

leoon.zhu@gmail.com

Zhejiang Cancer Hospital，Hangzhou Institute of Medicine (HIM), Chinese Academy of Sciences, Hangzhou, China.

Chuchu Zhang

Zhejiang Cancer Hospital，Hangzhou Institute of Medicine (HIM), Chinese Academy of Sciences, Hangzhou, China.

Danqing Yu

Zhejiang Cancer Hospital，Hangzhou Institute of Medicine (HIM), Chinese Academy of Sciences, Hangzhou, China.

Lili Zhou

Zhejiang Cancer Hospital，Hangzhou Institute of Medicine (HIM), Chinese Academy of Sciences, Hangzhou, China.

Qingping Zhong

Zhejiang Cancer Hospital，Hangzhou Institute of Medicine (HIM), Chinese Academy of Sciences, Hangzhou, China.

Jin Jiang

Affiliated Hospital of Jiaxing University, The First Hospital of Jiaxing

Zihao Jin

Zhejiang Cancer Hospital，Hangzhou Institute of Medicine (HIM), Chinese Academy of Sciences, Hangzhou, China.

Xu Qiu

Zhejiang Cancer Hospital，Hangzhou Institute of Medicine (HIM), Chinese Academy of Sciences, Hangzhou, China.

Jinggang Chen

Zhejiang Cancer Hospital，Hangzhou Institute of Medicine (HIM), Chinese Academy of Sciences, Hangzhou, China.

Jiang Zhu

Institute of feed science, college of animal science, Zhejiang university.

Zihan Mao

Cancer Hospital of China Medical University, Cancer Hospital of Dalian University of Technology, Liaoning Cancer Hospital & Institute, Shenyan, China

Minghua Bai

Zhejiang Cancer Hospital Hangzhou Institute of Medicine (HIM), Chinese Academy of Sciences, Hangzhou, China.

Article

Keywords: Colorectal cancer, TROP2 (TACSTD2), Radiotherapy resistance, Single-cell transcriptomics, Antibody-drug conjugate

Posted Date: July 20th, 2026

DOI: https://doi.org/10.21203/rs.3.rs-9879994/v1

License: This work is licensed under a Creative Commons Attribution 4.0 International License. Read Full License

Additional Declarations: (Not answered)

Abstract

Background

Radiotherapy is an important treatment modality for colorectal cancer (CRC), but intrinsic and acquired radioresistance remain major barriers to durable tumor control. Increasing evidence suggests that therapy resistance is shaped by heterogeneous malignant epithelial states and their interactions with the tumor microenvironment. However, the epithelial cell states associated with radiotherapy non-response in CRC and their therapeutic vulnerabilities remain poorly defined.

Objectives

This study aimed to identify malignant epithelial populations associated with radiotherapy resistance in CRC, define their biological characteristics, and determine whether these resistant states can be therapeutically targeted.

Methods

Patient-derived CRC single-cell RNA sequencing data were integrated and analyzed to characterize cellular composition, malignant epithelial subclusters, copy-number variation, pathway activity, differentiation trajectory, and cell–cell communication. TROP2/TACSTD2-associated epithelial states were further evaluated using survival analysis, enrichment analysis, pseudotime reconstruction, and ligand–receptor inference. Functional validation was performed in CRC cell models using TROP2 knockdown, TROP2 overexpression, clonogenic survival assays, immunofluorescence, western blotting, cell-cycle analysis, apoptosis assays, drug–radiation synergy analysis, and xenograft models treated with irradiation and sacituzumab govitecan (Trodelvy).

Results

Single-cell analysis identified a distinct TROP2^{+} malignant epithelial population enriched in radiotherapy non-responsive tumors and associated with poor prognosis. These cells occupied a terminally remodeled, stress-adapted epithelial state characterized by enhanced translation, oxidative metabolism, keratinocyte-like remodeling, and fibroblast-associated paracrine signaling. Functionally, TROP2 expression correlated with intrinsic radioresistance. TACSTD2 depletion sensitized CRC cells to irradiation, whereas TROP2 overexpression promoted radioresistance. Irradiation further induced TROP2 expression, creating a therapeutic vulnerability to Trodelvy. Combined irradiation and Trodelvy enhanced apoptosis, altered cell-cycle distribution, and suppressed tumor growth in xenograft models, particularly in radioresistant CRC.

Conclusion

TROP2 defines a stress-adapted malignant epithelial state that contributes to CRC radiotherapy resistance while providing an actionable therapeutic vulnerability. These findings support combined radiotherapy and TROP2-targeted antibody–drug conjugate treatment as a potential strategy to overcome radioresistance in CRC.

Introduction

Colorectal cancer (CRC) remains a major cause of cancer-related mortality worldwide[1]. Radiotherapy is a key component of multimodal treatment, particularly in locally advanced and rectal cancer, yet intrinsic and acquired resistance frequently limit durable tumor control[2, 3]. As a result, tumor persistence, local recurrence, and treatment failure remain substantial clinical challenges[4]. Despite its importance, the cellular basis of radiotherapy resistance in CRC is still incompletely understood[5, 6].

Increasing evidence indicates that treatment response is influenced not only by genetic alterations, but also by heterogeneous malignant epithelial states and their interactions with the tumor microenvironment; however, the epithelial states specifically associated with radiotherapy non-response in CRC remain poorly defined[7, 8].

Trophoblast cell surface antigen 2 (TROP2, encoded by TACSTD2) is a transmembrane glycoprotein broadly expressed in epithelial tissues and frequently upregulated in carcinomas[9, 10]. Beyond its value as a therapeutic target for antibody-drug conjugates such as sacituzumab govitecan, TROP2 has been linked to tumor progression and adverse prognosis across multiple epithelial malignancies[11, 12]. Yet whether TROP2 marks a distinct epithelial state associated with radioresistance in CRC, or actively contributes to the acquisition of such a phenotype, has not been systematically investigated[13].

Here, we integrated single-cell transcriptomic profiling of patient-derived CRC specimens with functional and pharmacologic validation to define epithelial states associated with radiotherapy response. We identify a distinct TROP2^{+} malignant epithelial population enriched in radiotherapy non-responsive tumors and show that these cells occupy a terminally remodeled, stress-adapted epithelial state characterized by enhanced translational activity, keratinocyte-like remodeling, and fibroblast-associated signaling. We further demonstrate that TROP2 functionally contributes to radiotherapy tolerance while simultaneously creating a therapeutic vulnerability to TROP2-targeted antibody-drug conjugate[14, 15]. Based on these findings, we propose a working model in which radiotherapy both selects for and induces TROP2-associated adaptive epithelial states that can be therapeutically exploited by combining radiotherapy with Trodelvy. These findings establish TROP2 as both a mechanistic determinant and a translational entry point for overcoming radiotherapy resistance in CRC.

Methods

Data availability

The single-cell RNA sequencing (scRNA-seq) data generated in this study were derived from patient CRC specimens collected at Zhejiang Cancer Hospital. Bulk RNA-seq data used for survival analyses were obtained from The Cancer Genome Atlas colorectal adenocarcinoma cohort (TCGA-COAD).

Single-cell RNA sequencing and data analysis

Tissue dissociation. Fresh colorectal cancer tissue samples were immediately processed for scRNA-seq. Tumor tissues and matched adjacent normal tissues were collected from patients undergoing surgical resection at Zhejiang Cancer Hospital. Single-cell suspensions for library construction were prepared through mechanical dissociation and enzymatic digestion. Briefly, tissue samples were transferred into a 60 × 15 mm culture dish, washed with pre-cooled D-PBS to remove blood and debris, and minced into small pieces of approximately 2-3 mm. The tissue fragments were then transferred into a 5 mL centrifuge tube, supplemented with 1 mL D-PBS, and further minced to approximately 1 mm. After three washes with D-PBS, tissues were incubated in Tumor Dissociation Kit, human (Miltenyi Biotec, cat. no. 130-095-929) digestion buffer at 37 °C and 100 rpm. An initial 5 mL of enzyme mix was used for digestion for 15 min, followed by gentle trituration with a Pasteur pipette and filtration through a 40 μm cell strainer. The remaining tissue fragments were then subjected to a second round of digestion with the remaining 5 mL enzyme mix for an additional 15 min, or longer if needed, until most tissue fragments were dissociated. Cell suspensions from the two rounds were combined and centrifuged at 400 × g, 4 °C, for 5 min. Residual erythrocytes were removed using 1× Red Blood Cell Lysis Solution at room temperature for 5 min, followed by washing with D-PBS and centrifugation at 400 × g, 4 °C, for 5 min. The final cell pellet was resuspended in RPMI 1640 medium and kept on ice. Cell concentration and viability were assessed using AO/PI staining and a Countstar cell counter. Cell suspensions were adjusted to a target concentration of 500-1,500 cells/μL, with cell viability > 80%, aggregation rate < 25%, and nucleated cell proportion in the suspension > 60%. Prepared cell suspensions were maintained on ice and subjected to single-cell capture within 30 min. When necessary, dead cells were further removed using the MACS® Dead Cell Removal Kit (Miltenyi Biotec, cat. no. 130-090-101) according to the manufacturer's instructions.

Single-cell capture, library preparation, and sequencing.

Single-cell suspensions were analyzed for viability and cell count prior to library construction. Single-cell capture, barcoding, and library preparation were performed using the SeekOne Digital Droplet System (M001A, SeekBio) and the SeekOne® DD Single-Cell 3' Transcriptome Kit (v2.3) according to the manufacturer's instructions. Cells were adjusted to 700-1,200 cells/μL, and approximately 20,000 cells were loaded per chip to generate Gel Beads-in-Emulsion (GEMs). Following reverse transcription, GEMs were broken for cDNA recovery, amplification, and purification. Amplified cDNA was fragmented, end-repaired, adapter-ligated, and PCR-amplified. Final libraries were quantified using a Qubit dsDNA HS Assay Kit and their fragment size distribution was assessed using Qsep100 High-Sensitivity DNA Chips.

Paired-end 150-bp sequencing was performed on the DNBSEQ-T7RS platform (MGI) or NovaSeq 6000 (Illumina).

Data preprocessing

Single-cell data analysis was performed using Seurat v5.3.0. Initial quality control involved filtering cells based on the following criteria: 1) more than 3 expressed cells,2) fewer than 200 total genes, 3) mitochondrial/ribosomal genes comprising over 20% of total gene expression, and 4) fewer than 200 or more than 10,000 detected RNA features. The "NormalizeData" function was employed to perform library size normalization and obtain normalized counts. Specifically, the "LogNormalize" method adjusted the gene expression measurements for each cell based on total expression, multiplied by a default scaling factor of 10,000, and log-transformed the results. Highly variable genes were identified using FindVariableFeatures, and the top 2,000 highly variable genes were used for downstream analyses. To remove batch effects in the scRNA-seq data, we utilized "harmony". The 30 top principal components were calculated based on the gene expression profiles of the highly variable genes. We selected an appropriate resolution for the "FindNeighbors" and "FindClusters" functions to perform cell clustering. In the integrated atlas shown in this study, clustering was performed at a resolution of 0.8. The "RunUMAP" function was used to visualize the initial clustering. We annotated the cells using the following canonical marker genes: endothelial cells (PECAM1, VWF), neutrophils (NAMPT, FCGR3B), dendritic cells (CD1A, HLA-DRA), T cells (CD3D, CD8A, CD4), NK cells (NKG7, GNLY, CD160), epithelial cells (EPCAM, KRT8, KRT18), fibroblasts (C1R, COL1A2, DCN, PDGFRA), B cells (CD79A), mast cells (TPSAB1, MS4A2), and monocytes (CD14, VCAN, FCGR3A, FCN1), macrophages (CD68, CD163, C1QB)[16]. Using the "FindAllMarkers" function in Seurat, we identified marker genes for each cluster, focusing only on positive markers relative to all other cells.

Patient samples

This study was approved by the Ethics Committee of Zhejiang Cancer Hospital and conducted in accordance with institutional ethical standards (IRB-2024-1085 (IIT)). Patients were classified into Naive, Response, and Non-Response groups according to radiotherapy exposure and clinical response criteria as defined in this study. Written informed consent was obtained from all patients prior to sample collection.

Subclustering of epithelial cells and definition of TROP2-based groups

Annotated epithelial cells were extracted from the integrated Seurat object and reanalyzed separately to resolve intra-epithelial heterogeneity. Tumor epithelial subclusters were identified by graph-based clustering and visualized by UMAP. Based on TACSTD2 expression across epithelial subclusters, malignant epithelial cells were classified into TROP2-high, TROP2-medium, and TROP2-low groups. For downstream binary analyses, cells assigned to the TROP2-high and TROP2-medium groups were merged and defined as $TROP2^{+}$ epithelial cells, whereas TROP2-low cells were defined as $TROP2^{-}$ epithelial cells. The relative abundance of these epithelial groups was compared across Naive, Response, and Non-

Response tumors. This TROP2-based binary grouping was used for downstream differential expression, pathway enrichment, and signaling activity analyses.

The copy number variation (CNV) analysis

The CNV evaluation of the epithelial cell subcluster in the tumor group was conducted using the "infercnv" R package (version 3.2.0) on the chromosome.We selected myeloid and CD8 T cells from normal adjacent tissue as references, setting the parameters denoise = TRUE and a cutoff value of 0.1, while keeping the remaining parameters at their defaults for the inferCNV analysis.

Enrichment analyses

Differential expression analysis between $TROP2^{+}$ and $TROP2^{-}$ epithelial cells was performed using the FindMarkers function in Seurat. Differentially expressed genes were identified using the Wilcoxon rank-sum test with min.pct = 0.1 and logfc.threshold = 0.25. For downstream enrichment analyses, significantly altered genes were further filtered using an adjusted P value < 0.05 and an absolute log2 fold change > 0.5. The clusterProfiler R package (version 4.18.4) was used to assess differential enrichment of KEGG and GO pathways between $TROP2^{+}$ and $TROP2^{-}$ epithelial cells. The PROGENy R package (version 1.28.0) was used to infer pathway activity. The UCell R package (version 2.8) was applied to calculate enrichment scores for the HALLMARK_EMT and GOBP_CELL_MIGRATION gene sets in epithelial cells.

Trajectory analyses

Trajectory analysis was performed using the Monocle2 R package (version 2.4.0) on $TROP2^{+}$ and $TROP2^{-}$ epithelial cells. Genes for trajectory inference were selected using the dispersionTable function, and only genes with a mean expression ≥0.1 were retained. Dimensionality reduction was performed using the reduceDimension function with the DDRTree method, with max_components = 3 and num_dim = 20. The CytoTRACE R package (version 0.3.3) was used to support root assignment in the pseudotime analysis. To identify genes associated with branch-dependent cell states, BEAM analysis was performed, and genes with a q value ≤0.01 were hierarchically clustered. Gene modules were further grouped using the ClusterGVis R package (version 0.1.2) with num_clusters = 4. GO enrichment analysis was subsequently performed to characterize the functional significance of the identified gene clusters.

Cell communication analysis of $TROP2^{+}$ malignant epithelial cells

The CellChat R package (version 2.1) was used to analyze global cell communication patterns between $TROP2^{+}$ and $TROP2^{-}$ epithelial cells. Subsequently, the MultiNicheNet R package (version 2.0.1) was applied to prioritize ligand–receptor interactions enriched in $TROP2^{+}$ epithelial cells. The NicheNet R package (version 2.2.0) was further used to infer downstream target genes associated with prioritized ligands, with JAK2 identified as a high-confidence target of HBEGF signaling.

Cell culture

Human CRC cell lines HCT8, HCT15, HCT116, HT29, SW480, SW620, and RKO were used for baseline expression analysis, whereas SW480, HCT116, and a radioresistant derivative of HCT116 cells (HCT116 RR) were used for functional validation. Cells were cultured in Dulbecco's Modified Eagle Medium (DMEM) supplemented with 10% fetal bovine serum and 1% penicillin/streptomycin, and maintained at 37 °C in a humidified incubator with 5% CO_2.

Irradiation

For irradiation experiments, cells were exposed to graded doses of ionizing radiation ranging from 0 to 6 Gy. For radiation-induction experiments, HCT116 cells were harvested at serial time points from 1 to 48 h after irradiation at 2, 4, or 6 Gy. For drug treatment experiments, cells were treated with Trodelvy either alone or in combination with irradiation. In apoptosis assays, Trodelvy was used at 50 ng/mL in combination with 4 Gy irradiation.

Lentiviral constructs and transduction

To knock down TACSTD2, shRNA sequences targeting TACSTD2 were cloned into the pLKO.1-puro vector, while a non-targeting shRNA served as the negative control. The shRNA target sequences used in this study are listed in Supplementary Table S1. For overexpression studies, the full-length coding sequence of TACSTD2 was inserted into the pCDH-CMV-MCS-EF1-copGFP-T2A-Puro lentiviral expression vector, and the corresponding empty vector served as the control[17]. For lentiviral particle generation, 293T cells were co-transfected with the lentiviral transfer vector together with the packaging plasmids psPAX2 and pMD2.G using LipoX Plus Reagent. Viral supernatants were collected 48 h after transfection and used to infect target colorectal cancer cells. Following viral infection, stable polyclonal cell populations were established by puromycin-based antibiotic selection and validated by western blotting prior to downstream experiments.

Western blotting

Western blotting was performed according to a standard protocol. Briefly, whole-cell lysates were prepared using RIPA lysis buffer supplemented with protease inhibitors, and protein concentrations were determined using a BCA protein assay kit. Equal amounts of protein were separated by SDS-PAGE and transferred onto PVDF membranes. Membranes were blocked with 5% non-fat milk and incubated overnight at 4 °C with primary antibodies, including anti-TROP2 antibody (cat. no. ab214488) and, where indicated, anti-phospho-Histone H2A.X (S139) antibody (cat. no. ab81299), followed by incubation with HRP-conjugated secondary antibodies. β-actin was used as the loading control. Signals were detected using an enhanced chemiluminescence (ECL) system.

Immunofluorescence

Cells were seeded onto confocal imaging dishes and cultured overnight. The cells were then fixed with 4% paraformaldehyde for 15 min, permeabilized with 0.2% Triton X-100 for 15 min, and blocked with 5% bovine serum albumin (BSA) for 1 h at room temperature. Cells were subsequently incubated with anti-TROP2 primary antibody overnight at 4 °C, followed by incubation with fluorophore-conjugated secondary antibodies for 1 h at room temperature in the dark. Nuclei were counterstained with DAPI, and images were acquired using a Leica confocal microscope.

Colony formation assay

Radiosensitivity was assessed by clonogenic survival assay. Cells were seeded into 6-well plates at appropriate densities according to the radiation dose and allowed to attach overnight. Cells were then exposed to 0, 2, 4, or 6 Gy ionizing radiation and cultured for 10 days to allow colony formation. Colonies were fixed with 4% paraformaldehyde and stained with 1% crystal violet. Colonies containing at least 50 cells were counted as surviving colonies. Plating efficiency (PE) was calculated as the number of colonies formed divided by the number of cells seeded, and the surviving fraction (SF) at each radiation dose was calculated by normalizing to the plating efficiency of the non-irradiated control. Clonogenic assays were used to compare intrinsic radiosensitivity across CRC cell lines and to evaluate the effects of TACSTD2 knockdown or overexpression on radiation response. Survival curves were plotted using GraphPad Prism according to standard radiobiological Animal experiments[18].

Animal models

All animal experiments were performed in accordance with institutional guidelines and approved by the relevant animal ethics committee. HCT116 WT or HCT116 RR cells were subcutaneously injected into the flanks of immunodeficient mice. When the average tumor volume reached approximately 100 mm^3, mice were randomly assigned to treatment groups. Tumor-bearing mice received local irradiation at 8 Gy per fraction for three consecutive days, Trodelvy at 25 mg/kg three times per week, or the combination of irradiation and Trodelvy[19, 20]. Tumor length and width were measured every 2–3 days using calipers, and tumor volume was calculated using the formula: volume = length × $width^2$ / 2. At the study endpoint, tumors were harvested, photographed, and subjected to downstream analysis where applicable.

Drug response and synergy analysis

To evaluate the combined effect of Trodelvy and irradiation, HCT116 cells were treated with increasing concentrations of sacituzumab govitecan in combination with graded doses of ionizing radiation, as shown in the response-surface analysis in the Results. The resulting cell viability matrix was analyzed using Combenefit 2.021 according to the Bliss, highest single agent (HSA), and Loewe reference models, and response-surface plots were generated to visualize combination effects[15].

Flow cytometric analysis of cell cycle and apoptosis

Cell-cycle distribution and apoptosis were analyzed by flow cytometry. For cell-cycle analysis, CRC cells were treated with irradiation, Trodelvy, or their combination as indicated. After treatment, cells were harvested, washed twice with PBS, and fixed in 70% ice-cold ethanol at 4 °C overnight. Fixed cells were then washed with PBS and incubated with RNase A-containing propidium iodide (PI) staining solution according to the manufacturer's instructions. Samples were analyzed by flow cytometry. Debris and cell aggregates were excluded using FSC/SSC gating and single-cell discrimination based on PI-A versus PI-H parameters. DNA-content histograms were modeled using ModFit LT 5.0, and the proportions of cells in G0/G1, S, and G2/M phases were quantified. Quantitative results were summarized from three independent replicates and plotted using GraphPad Prism. For apoptosis analysis, wild-type HCT116 and radioresistant HCT116 RR cells were treated with 4 Gy irradiation, Trodelvy at 50 ng/mL, or the combination of both. After 72 h of treatment, cells were harvested, washed twice with PBS, and stained using an Annexin V-FITC/PI apoptosis detection kit according to the manufacturer's instructions. Samples were analyzed on a Sony flow cytometer, and apoptotic fractions were quantified using FlowJo software. $FITC^-/PI^-$ cells were considered viable cells, $FITC^+/PI^-$ cells were considered early apoptotic cells, and $FITC^+/PI^+$ cells were considered late apoptotic or dead cells. The total apoptotic fraction was calculated as the sum of early and late apoptotic cells.

Statistical analysis

All statistical analyses were conducted using R (version 4.3.0) and Graphpad Prism 7 (version 7.0). UMAP was used for dimensionality reduction analysis. Wilcoxon test was used to compare differences between two groups, while Kruskal-Wallis's test was used to compare differences among multiple groups. Survival curves were compared by log-rank test, and Cox proportional hazards models were used for survival regression analyses. Statistical p-values were calculated as two-sided, with $p < 0.05$ deemed statistically significant.

Results

sc-RNA profiling of CRC

The overall rationale and workflow of this study are summarized in Fig. 1A. Briefly, patient-derived single-cell transcriptomes were used to identify a $TROP2^+$ malignant epithelial population enriched in radiotherapy non-responsive CRC. We then characterized this population as a terminally remodeled, stress-adapted epithelial state, evaluated its functional role in radioresistance, and tested whether radiation-induced TROP2 expression could be therapeutically exploited using the TROP2-targeted antibody–drug conjugate sacituzumab govitecan (Trodelvy) (Fig. 1A). To delineate the cellular architecture associated with differential radiotherapy outcomes in colorectal cancer, we performed single-cell RNA sequencing on CRC samples from three clinical groups, including Naive, Response, and Non-Response tumors. After stringent quality control and integration, a total of 78,929 high-quality cells were retained for downstream analysis[21]. Dimensionality reduction using the top 30 principal components at a clustering resolution of 0.8 resolved the major cellular populations within the CRC

microenvironment (Fig. 1B). Batch-corrected UMAP embedding showed effective batch mixing across patients, supporting the comparability of downstream analyses across clinical groups (Fig. 1C).

Given the central role of epithelial plasticity in treatment response, we next examined the distribution of TACSTD2 across the integrated atlas. TROP2 expression was not uniformly distributed, but was instead enriched in discrete epithelial regions of the UMAP, suggesting the presence of transcriptionally distinct epithelial subpopulations (Fig. 1D). We then quantified the relative abundance of major cell compartments across the three clinical groups and observed clear differences in epithelial, immune, and stromal composition among Naive, Response, and Non-Response tumors (Fig. 1E). Canonical markers for each cell type are shown in Fig. S1, their distribution across the UMAP is presented in Fig. 1F, and the top markers for each population are shown in Fig. S2. Together, these data establish a single-cell atlas of CRC under radiotherapy and identify a TROP2-enriched epithelial compartment as a candidate population associated with treatment response and tumor evolution.

TROP2^{+} malignant epithelial cells are enriched in radiotherapy non-responsive CRC and associated with adverse outcome

Because the integrated atlas pointed to epithelial heterogeneity as a prominent feature of radiotherapy-associated variation, we next focused specifically on the epithelial compartment. Epithelial cells were subsetted for re-clustering, revealing multiple transcriptionally distinct epithelial subclusters (Fig. 2A). To determine their malignant nature, we performed inferCNV analysis using CD8^{+} T cells and Myeloid cells from matched adjacent normal tissues as references. This analysis demonstrated marked copy-number alterations across multiple epithelial subclusters, whereas reference populations showed minimal CNV signal, validating the malignant identity of the epithelial populations and revealing heterogeneity in genomic instability across subclusters (Fig. 2B and C).

We then compared epithelial subcluster distributions across Naive, Response, and Non-Response tumors. Non-Response tumors were preferentially enriched for specific epithelial states, suggesting that radiotherapy-resistant tumors harbor distinct epithelial programs (Fig. 2D). Because TROP2 expression had already emerged as a prominent feature of the epithelial compartment in the integrated atlas, we next mapped TACSTD2 expression across epithelial subclusters. TACSTD2 expression was highly concentrated in cluster 6 and present at an intermediate level in cluster 1, whereas other epithelial subclusters showed minimal expression (Fig. 2E–G). Based on this distribution, cluster 6 was defined as the TROP2-high population, cluster 1 as the TROP2-medium population, and the remaining epithelial subclusters as TROP2-low populations. For downstream binary analyses, TROP2-high and TROP2-medium cells were collectively defined as TROP2^{+} malignant epithelial cells, whereas TROP2-low cells were defined as TROP2^{-} malignant epithelial cells. Importantly, the proportion of TROP2^{+} malignant epithelial cells was markedly increased in non-response tumors, whereas response tumors contained only a minor TROP2^{+} fraction (Fig. 2H).

To assess the clinical relevance of this TROP2-associated epithelial state, we analyzed bulk TCGA-COAD data. Kaplan–Meier analysis showed that patients with high TACSTD2 expression had significantly worse overall survival than those with low TACSTD2 expression (log-rank P = 0.011; Fig. 2I). Cox regression analysis further supported elevated TACSTD2 expression as an adverse prognostic factor. In parallel, differential expression analysis demonstrated marked transcriptional divergence between $TROP2^{+}$ and $TROP2^{-}$ malignant epithelial cells (Fig. 2J). Together, these findings indicate that CRC contains transcriptionally and genomically distinct epithelial populations, and that $TROP2^{+}$ malignant epithelial cells define a clinically relevant malignant state enriched in radiotherapy non-responsive tumors[9].

$TROP2^{+}$ malignant epithelial cells occupy a terminally remodeled state with enhanced translational and metabolic activity

Having identified $TROP2^{+}$ malignant epithelial cells as a treatment-relevant epithelial population, we next sought to define their biological properties. KEGG enrichment analysis showed that $TROP2^{+}$ malignant epithelial cells were enriched for cornified envelope formation and oxidative phosphorylation (Fig. 3A). Gene Ontology analysis further revealed enrichment of cytoplasmic translation, epidermis development, keratinocyte differentiation, and ribosome biogenesis (Fig. 3B), suggesting that $TROP2^{+}$ malignant epithelial cells are characterized by enhanced translational activity and keratinocyte-like remodeling. Consistently, supplementary GSVA and enrichment analyses further showed that TROP2-associated epithelial subgroups exhibited broad differences in HALLMARK pathway activity, including cell-cycle-, stress-response-, metabolic-, and apoptosis-related programs (Supplementary Fig. S3 and S4). Extended GO and KEGG analyses provided additional support for the enrichment of epithelial remodeling, metabolic, and stress-adaptive pathways in the TROP2-associated state (Supplementary Fig. S5 and S6).

To explore upstream signaling activity, we performed PROGENy analysis and found that $TROP2^{+}$ malignant epithelial cells exhibited increased activation of EGFR, p53, MAPK, TGF-β, TNF-α, and JAK–STAT pathways relative to $TROP2^{-}$ malignant epithelial cells (Fig. 3C). In addition, UCell-based scoring revealed modest but consistent enrichment of EMT- and migration-related signatures in $TROP2^{+}$ malignant epithelial cells (Fig. 3D and E), suggesting that this population retains features of partial epithelial plasticity and enhanced migratory potential. Collectively, these results indicate that $TROP2^{+}$ malignant epithelial cells are not simply defined by marker expression, but instead represent a distinct epithelial program characterized by enhanced translational activity, keratinocyte-like remodeling, and oxidative metabolism.

To determine the position of $TROP2^{+}$ malignant epithelial cells along the epithelial differentiation continuum, we performed pseudotime analysis. This reconstruction resolved a branched epithelial trajectory (Fig. 3F and G). CytoTRACE scoring indicated that the highest differentiation potential was

located around the intermediate region near the branch point rather than at the earliest pseudotime positions (Fig. 3H), suggesting that the epithelial hierarchy in this dataset does not conform to a simple early-to-late linear stemness model.

Mapping TROP2^{+} and TROP2^{-} malignant epithelial cells onto the trajectory revealed a striking spatial segregation. TROP2^{-} malignant epithelial cells occupied multiple early and intermediate states spanning pseudotime 0–12, whereas TROP2^{+} malignant epithelial cells formed a highly concentrated terminal cluster around pseudotime 15–18 (Fig. 3H and I). Density analysis further showed a sharp unimodal peak of TROP2 expression specifically within the 15–18 pseudotime window, with little to no signal in earlier states (Fig. 3J). These findings support the view that TROP2^{+} malignant epithelial cells correspond to a differentiated, metabolically active, and injury-responsive terminal state rather than a classical early stem-like compartment.

To further characterize branch-dependent transcriptional programs associated with the trajectory leading to the TROP2^{+} terminal state, we performed BEAM analysis along the epithelial trajectory. Four gene modules associated with distinct branch dynamics were identified (Fig. 3K). Module 4 was enriched for epidermis development and keratinocyte differentiation, consistent with terminal epithelial remodeling. Module 3 captured metabolic and growth-regulatory programs, whereas Module 2 was associated with vesicle-mediated transport and RNA processing. Module 1 was characterized by ribosomal and translational machinery. Together, these findings suggest that TROP2^{+} malignant epithelial cells occupy a terminal epithelial state characterized by enhanced translation, metabolic activation, and keratinization-related remodeling during CRC epithelial evolution.

Cell communication characteristics of TROP2^{+} malignant epithelial cells

Because terminal epithelial states often depend on sustained microenvironmental support, we next investigated whether TROP2 status was associated with altered cell communication. Using MultiNicheNet algorithm, we found that TROP2 + malignant epithelial cells displayed both a higher number of inferred interactions and stronger overall communication intensity than TROP2- malignant epithelial cells (Fig. 4A and B), suggesting that the TROP2-associated epithelial state is embedded within a more communication-active tumor microenvironment. Interaction mapping further showed that TROP2^{+} malignant epithelial cells exhibited particularly strong outgoing signaling toward fibroblasts, endothelial cells, and myeloid populations (Fig. 4C).

At the ligand-receptor level, TROP2^{+} malignant epithelial cells showed stronger signaling with fibroblasts through the HBEGF-EGFR, CLCF1-LIFR, and CLCF1-IL6ST axes, together with higher inferred ligand activity (Fig. 4D). Among these, HBEGF was robustly upregulated in TROP2^{+} malignant epithelial cells, and NicheNet identified JAK2 as a high-confidence downstream target, supporting activation of EGFR-centered JAK/STAT inflammatory-survival signaling.. By contrast, CLCF1 showed only limited ligand-target coupling and lacked clearly enriched downstream targets, suggesting that its contribution in this

context may be indirect or weaker at the transcriptional level (Fig. 4E and F). These findings indicate that TROP2^{+} malignant epithelial cells occupy a signaling-active niche and that EGFR-centered fibroblast-epithelial crosstalk may help reinforce survival, inflammation, and tissue remodeling in radiotherapy-resistant CRC[22].

TROP2 promotes intrinsic radioresistance in CRC cells

To determine whether TROP2 is functionally contributes to radiotherapy resistance, rather than simply marking a resistant epithelial state, we next performed in vitro validation in CRC cell models. Western blot analysis across a panel of CRC cell lines revealed heterogeneous basal TROP2 expression, with SW480 cells displaying the highest baseline abundance, whereas HCT8, HCT15, HT29, SW620, and RKO cells exhibited low or undetectable levels (Fig. 5A). We then assessed clonogenic survival following graded irradiation. Both SW480 cells and an HCT116 radioresistant derivative (HCT116 RR) showed significantly higher surviving fractions than parental HCT116 cells across 0–6 Gy (Fig. 5B and D). Consistently, immunofluorescence staining demonstrated markedly increased membrane TROP2 expression in HCT116 RR cells relative to wild-type HCT116 cells (Fig. 5C).

To further examine whether TROP2 expression influences cellular response to irradiation, we genetically manipulated TROP2 expression in CRC cells. Stable shRNA-mediated knockdown of TACSTD2 in SW480 cells substantially reduced TROP2 protein levels (Fig. 5E and F), whereas lentiviral overexpression in HCT116 cells markedly increased TROP2 abundance (Fig. 5H and I). Cell-cycle analysis further showed that TACSTD2 knockdown in SW480 cells altered radiation-associated cell-cycle distribution, particularly under irradiated conditions, whereas TROP2 overexpression in HCT116 cells reshaped cell-cycle distribution following irradiation (Fig. 5G and J). These findings suggest that TROP2 expression is associated with intrinsic radioresistance and may influence the cellular adaptation of CRC cells to radiation-induced stress.

Radiation-induced TROP2 expression sensitizes CRC cells to ADC treatment

Having established a functional role for TROP2 in intrinsic radioresistance, we next asked whether irradiation itself regulates TROP2 and whether this induced state can be therapeutically exploited. Time-course western blotting in HCT116 cells showed that TROP2 protein levels were dynamically induced following exposure to 2, 4, or 6 Gy ionizing radiation, with gradual upregulation over 1–48 h that was most pronounced at intermediate doses (Fig. 6A). Immunofluorescence staining further confirmed that 4 Gy irradiation markedly increased membrane-localized TROP2 in wild-type HCT116 cells relative to non-irradiated controls (Fig. 6B). These results indicate that TROP2 is not only a pre-existing marker of resistant epithelial states, but also an inducible component of the cellular response to radiation.

We next asked whether this radiation-induced TROP2 state could be therapeutically exploited using the antibody–drug conjugate Trodelvy. Response-surface synergy analysis showed that increasing Trodelvy concentration together with escalating radiation dose cooperatively reduced the viability of HCT116

cells, consistent with a synergistic interaction between the two treatments (Fig. 6C). Flow-cytometric apoptosis analysis further demonstrated that in both wild-type HCT116 and HCT116 RR cells, either 4 Gy irradiation alone or Trodelvy alone induced only modest apoptosis, whereas the combination of 4 Gy plus Trodelvy markedly increased apoptotic fractions (Fig. 6D-G). Notably, this effect was more pronounced in the radioresistant HCT116 RR line. These data indicate that radiation not only induces TROP2 expression, but also renders CRC cells more vulnerable to ADC treatment, with Trodelvy acting as an effective radiosensitizer particularly in TROP2-high, radioresistant CRC cells[23].

Genetic targeting of TROP2 and Trodelvy-based combination therapy suppress CRC radioresistance in vitro and in vivo

To directly test the functional consequence of TROP2 gain or loss during radiation response, we next performed clonogenic assays in genetically modified CRC cells. In HCT116 cells, TROP2 overexpression increased clonogenic survival following irradiation compared with vector controls, supporting a role for TROP2 in promoting radioresistance. Conversely, TACSTD2 knockdown in SW480 cells reduced clonogenic survival after irradiation compared with negative-control cells, indicating that endogenous TROP2 is required for maintaining the radioresistant phenotype in TROP2-high CRC cells (Fig. 7B and C).

We then examined whether pharmacological targeting of TROP2 with Trodelvy was accompanied by cell-cycle redistribution under irradiation. Representative propidium iodide DNA-content histograms showed distinct changes in G0/G1, S, and G2/M phase distribution after treatment with control, Trodelvy, irradiation, or irradiation plus Trodelvy (Fig. 7D). Quantitative analysis confirmed treatment-associated redistribution of cell-cycle phases, with Trodelvy-containing groups showing increased G2/M fractions compared with control conditions and the combined treatment maintaining a redistributed profile under irradiation (Fig. 7E). These data suggest that cell-cycle redistribution represents one component of the cellular response associated with TROP2-targeted therapy and irradiation.

To determine whether the therapeutic interaction between irradiation and Trodelvy extends to in vivo tumor control, we established CRC xenograft models using HCT116 WT and HCT116 RR cells. Once tumors reached approximately 100 mm^3, mice were randomized into treatment groups and treated with local irradiation, Trodelvy, or the combination according to the experimental schedule (Fig. 7A). At the study endpoint, tumors from the combination-treated group were visibly smaller than those from irradiation alone or other treatment groups (Fig. 7F). In HCT116 WT xenografts, irradiation alone delayed tumor growth and Trodelvy alone produced a moderate inhibitory effect, whereas the combination of irradiation and Trodelvy resulted in the strongest suppression of tumor growth throughout the treatment period (Fig. 7G). A similar but more striking pattern was observed in HCT116 RR xenografts, in which irradiation alone only partially delayed tumor progression, while irradiation plus Trodelvy markedly suppressed tumor growth (Fig. 7H).

These results demonstrate that TROP2 functionally promotes CRC radioresistance, while radiation-induced or pre-existing TROP2 expression creates an ADC-targetable vulnerability that can be exploited by combining radiotherapy with Trodelvy, including in radioresistant CRC xenograft models.

Discussion

Radiotherapy remains a cornerstone in the management of colorectal cancer, yet intrinsic and acquired resistance continues to limit its clinical efficacy. Although prior studies have largely emphasized genomic alterations or bulk transcriptional signatures associated with radioresistance, the malignant epithelial states and microenvironmental interactions that sustain this phenotype have remained insufficiently defined[24]. By integrating single-cell transcriptomics with functional validation, our study identifies TROP2^{+} malignant epithelial cells as a clinically relevant epithelial population enriched in radiotherapy non-responsive tumors and functionally linked to radiotherapy resistance[25].

A major conceptual advance of this study is that TROP2 does not simply label a resistant subset, but rather marks a distinct epithelial state with coordinated biosynthetic, structural, and adaptive features. TROP2^{+} malignant epithelial cells were characterized by enhanced translational activity, ribosome biogenesis, keratinocyte-like remodeling, and oxidative metabolism, collectively defining a metabolically active and structurally reinforced phenotype[26]. This interpretation is consistent with emerging evidence that mitochondrial energy metabolism, tumor hypoxia, and therapy-induced immune checkpoint remodeling can shape radiotherapy response and influence the efficacy of radiosensitizing strategies[27]. This state differs from the conventional view that treatment resistance is primarily driven by stem-like or highly proliferative tumor populations. Instead, our data support the idea that radiotherapy resistance in CRC may also emerge from a differentiated but stress-adapted epithelial state with increased biosynthetic and repair capacity[28].

Trajectory-based analyses further positioned TROP2^{+} malignant epithelial cells at the terminal end of the epithelial continuum. Both pseudotime reconstruction and CytoTRACE analysis argued against a classical progenitor-like identity and instead supported a terminally remodeled epithelial fate. Importantly, branch-associated transcriptional programs indicated that this state is coupled to keratinization, RNA processing, metabolic adaptation, and translational reinforcement[29]. Together, these findings suggest that radioresistance in CRC is not exclusively linked to developmental immaturity, but can also arise through alternative epithelial differentiation trajectories that culminate in a stress-adapted terminal state.

Our results also indicate that this TROP2-associated epithelial state is not maintained solely by cell-intrinsic programs[30]. Cell communication analyses identified strengthened fibroblast–epithelial interactions, with HBEGF–EGFR signaling emerging as a prominent candidate axis and JAK2 inferred as a high-confidence downstream target. Given the established role of EGFR-centered signaling in epithelial survival, inflammatory signaling, and DNA damage adaptation, these observations support a model in which stromal-derived cues may help reinforce the resistant phenotype of TROP2^{+} malignant epithelial cells under therapeutic stress[31]. Because this axis was inferred from computational ligand–receptor and target prediction analyses, further experimental validation will be required to define its causal contribution.

Functionally, our in vitro data move TROP2 beyond correlation and establish it as a contributor to the resistant phenotype. Basal TROP2 expression correlated with intrinsic radioresistance across CRC cell models, and HCT116 RR cells displayed higher TROP2 expression than parental HCT116 cells. Genetic depletion of TACSTD2 increased radiosensitivity, whereas enforced expression conferred resistance, indicating that TROP2 is not merely a passive marker of a pre-existing state. Equally important, ionizing radiation itself induced TROP2 expression, suggesting that radiotherapy may actively reinforce or expand this adaptive epithelial program. This inducibility provides a mechanistic bridge between treatment exposure and the emergence of resistant cell states, and may help explain how initially heterogeneous tumors become enriched for therapy-tolerant epithelial populations during treatment.

From a translational perspective, the most clinically actionable implication of our study is that the same epithelial state associated with radiation resistance also exposes a therapeutic vulnerability[32]. Trodelvy synergized with irradiation, enhanced apoptosis, altered treatment-associated cell-cycle distribution, and suppressed tumor growth in xenograft models, particularly in radioresistant CRC[33]. These findings suggest a potentially useful therapeutic logic: radiotherapy may induce or enrich a TROP2-high adaptive state, whereas ADC treatment may then preferentially target this otherwise resistant population[18]. In this sense, TROP2 represents both a mechanistic determinant of resistance and a therapeutic entry point for combination strategies[34].

Our findings support a model in which radiotherapy resistance in CRC is mediated, at least in part, by the emergence of a TROP2-associated, terminally remodeled epithelial state sustained by both intrinsic transcriptional programs and extrinsic microenvironmental cues[35]. Enhanced biosynthetic activity, structural reinforcement, adaptive signaling, and inducible TROP2 expression together may allow these cells to better tolerate genotoxic stress. This model not only expands the biological framework through which CRC radioresistance can be understood, but also provides a mechanistic rationale for combining radiotherapy with ADC-based treatment to overcome adaptive resistance[36].

Several limitations should be acknowledged. First, the number of patient samples analyzed at single-cell resolution remains limited, and larger cohorts will be necessary to establish the robustness and generalizability of the identified epithelial state. Second, although our analyses implicate fibroblast-associated signaling and the HBEGF–EGFR–JAK2 axis, these interactions were inferred computationally and require direct functional validation. Third, although the combination of radiotherapy and Trodelvy showed encouraging activity in cell and xenograft models, additional studies are needed to define optimal treatment scheduling, dose dependence, toxicity, and clinical applicability[26]. Finally, the precise downstream molecular mechanisms by which TROP2 regulates DNA damage tolerance, cell-cycle adaptation, and apoptotic response remain to be further dissected[37, 38].

In conclusion, this study identifies a TROP2-associated epithelial state as a mechanistic basis and therapeutic vulnerability of radiotherapy resistance in CRC[39, 40]. These findings provide a framework for understanding how epithelial plasticity, stromal support, and treatment-induced adaptation converge to shape radiotherapy response, and they support further evaluation of radiotherapy–ADC combination

strategies in resistant CRC[41]. Nevertheless, the clinical efficacy of TOP1 inhibitor-based ADCs may be constrained by target heterogeneity, multidrug resistance, and payload-related resistance, and next-generation ADC platforms using alternative TOP1 payloads such as exatecan have shown the potential to overcome resistance in colon and lung cancer models[15, 42].

Declarations

Conflict of interest disclosure

The authors declare that they have no competing interests.

Funding statement

This work was supported by the National Natural Science Foundation of China [No. 82574019], Central Government Guiding Local Science and Technology Development Fund [No. 2025ZY01060], Zhejiang Provincial “Vanguard and Leading Goose+X” Science and Technology Program [No. 2026C02A1095], Jiaxing Key Research and Development Program [No. 2024BZ20004], National Clinical Key Specialty Construction Project-Oncology department [No.2023-GJZK-001], BeijingXisike Clinical Oncology Research Foundationy [Y-Gilead2024-PT-0092].

Author contributions

Chuchu Zhang, Danqing Yu, and Lili Zhou contributed equally to this work. Chuchu Zhang, Danqing Yu, and Lili Zhou conceived the study, performed data analysis, interpreted the results, and drafted the manuscript. Qingping Zhong contributed to data analysis, figure preparation, and manuscript revision. Jinggang Chen was primarily responsible for the experimental validation and contributed to data acquisition and interpretation. Zihao Jin, Xu Qiu and Jiang Zhu contributed to sample processing, experimental support, data organization, and manuscript discussion. Zihan Mao and Minghua Bai supervised the study and provided critical revisions to the manuscript. Ji Zhu conceived and supervised the project, guided the overall study design and data interpretation, and revised the manuscript. All authors reviewed and approved the final manuscript.

Ethics approval statement

This study was approved by the Institutional Review Board of the Zhejiang Cancer Hospital (IRB-2024-1085 (IIT)). The study was performed in accordance with the Helsinki Declaration and Rules of Good Clinical Practice. All participants signed written informed consents after full explanation.

Acknowledgements

The authors acknowledge the support from the Shared Instrumentation Core Facility at the Hangzhou Institute of Medicine (HIM), Chinese Academy of Sciences, for providing the experimental platform and

technical assistance. We thank Cosmos Wisdom biotech co. ltd (Hangzhou. China), Dr Yating Zhang and Dr Xiaozhen Chen for scRNA-seq technical support.

Data Availability

The method section describes all the data utilized for analysis and processing in this study. On reasonable request, the corresponding author will provide the data and code supporting the conclusions of this work.

References

1. Li, N., et al., *Incidence, mortality, survival, risk factor and screening of colorectal cancer: A comparison among China, Europe, and northern America.* Cancer Lett, 2021. **522**: p. 255-268.
2. Tan, G., et al., *Radiosensitivity of colorectal cancer and radiation-induced gut damages are regulated by gasdermin E.* Cancer Lett, 2022. **529**: p. 1-10.
3. Mu, P., et al., *Unveiling radiobiological traits and therapeutic responses of BRAF(V600E)-mutant colorectal cancer via patient-derived organoids.* J Exp Clin Cancer Res, 2025. **44**(1): p. 92.
4. Andrei, P., et al., *Integrated approaches for precision oncology in colorectal cancer: The more you know, the better.* Semin Cancer Biol, 2022. **84**: p. 199-213.
5. Meng, Y., et al., *Salt-inducible kinase 2 confers radioresistance in colorectal cancer by facilitating homologous recombination repair.* MedComm (2020), 2025. **6**(2): p. e70083.
6. Wang, Y., et al., *HSP90 regulates dCK stability and inhibits ionizing radiation-induced ferroptosis in cervical cancer cells.* Cell Death Discovery, 2025. **11**(1).
7. Chu, X., et al., *Integrative single-cell analysis of human colorectal cancer reveals patient stratification with distinct immune evasion mechanisms.* Nat Cancer, 2024. **5**(9): p. 1409-1426.
8. Qi, J., et al., *Single-cell and spatial analysis reveal interaction of FAP(+) fibroblasts and SPP1(+) macrophages in colorectal cancer.* Nat Commun, 2022. **13**(1): p. 1742.
9. Morgenstern-Kaplan, D., et al., *Genomic, immunologic, and prognostic associations of TROP2 (TACSTD2) expression in solid tumors.* Oncologist, 2024. **29**(11): p. e1480-e1491.
10. Qiu, S., et al., *Targeting Trop-2 in cancer: Recent research progress and clinical application.* Biochim Biophys Acta Rev Cancer, 2023. **1878**(4): p. 188902.
11. Wen, Y., et al., *A literature review of the promising future of TROP2: a potential drug therapy target.* Ann Transl Med, 2022. **10**(24): p. 1403.
12. Lenart, S., et al., *Trop2: Jack of All Trades, Master of None.* Cancers (Basel), 2020. **12**(11).
13. Svec, J., et al., *TROP2 Represents a Negative Prognostic Factor in Colorectal Adenocarcinoma and Its Expression Is Associated with Features of Epithelial-Mesenchymal Transition and Invasiveness.* Cancers (Basel), 2022. **14**(17).
14. Liu, X., et al., *Trop2-targeted therapies in solid tumors: advances and future directions.* Theranostics, 2024. **14**(9): p. 3674-3692.

15. Weng, W., et al., *Antibody-Exatecan Conjugates with a Novel Self-immolative Moiety Overcome Resistance in Colon and Lung Cancer.* Cancer Discov, 2023. **13**(4): p. 950-973.
16. Liu, Y., et al., *Immune phenotypic linkage between colorectal cancer and liver metastasis.* Cancer Cell, 2022. **40**(4): p. 424-437.e5.
17. Goldenberg, D.M., et al., *Trop-2 is a novel target for solid cancer therapy with sacituzumab govitecan (IMMU-132), an antibody-drug conjugate (ADC).* Oncotarget, 2015. **6**(26): p. 22496-512.
18. Chen, Y.F., et al., *SNX10 deficiency impairs sensitivity to anti-HER2 antibody-drug conjugates via altering HER2 trafficking in HER2-positive breast cancer.* Proc Natl Acad Sci U S A, 2025. **122**(16): p. e2417586122.
19. Bardia, A., et al., *Sacituzumab Govitecan in Metastatic Triple-Negative Breast Cancer.* N Engl J Med, 2021. **384**(16): p. 1529-1541.
20. Chang, W.I., et al., *PI3Kalphadelta Inhibitor Combined With Radiation Enhances the Antitumor Immune Effect of Anti-PD1 in a Syngeneic Murine Triple-Negative Breast Cancer Model.* Int J Radiat Oncol Biol Phys, 2021. **110**(3): p. 845-858.
21. E, H., et al., *SNAI1 promotes epithelial-mesenchymal transition and maintains cancer stem cell-like properties in thymic epithelial tumors through the PIK3R2/p-EphA2 Axis.* J Exp Clin Cancer Res, 2024. **43**(1): p. 324.
22. Wang, Y., et al., *Single-cell multi-omics reveals that FABP1 + renal cell carcinoma drive tumor angiogenesis through the PLG-PLAT axis under fatty acid reprogramming.* Mol Cancer, 2025. **24**(1): p. 179.
23. *<Activity of Enfortumab Vedotin and Sacituzumab Govitecan with Radiation in Preclinical Models of Bladder Cancer.pdf>*.
24. Foersch, S., et al., *TROP2 in colorectal carcinoma: associations with histopathology, molecular phenotype, and patient prognosis.* J Pathol Clin Res, 2024. **10**(5): p. e12394.
25. Guerra, E., et al., *Trop-2, Na(+)/K(+) ATPase, CD9, PKCalpha, cofilin assemble a membrane signaling super-complex that drives colorectal cancer growth and invasion.* Oncogene, 2022. **41**(12): p. 1795-1808.
26. Hong, W.F., et al., *Dynamic immunoediting by macrophages in homologous recombination deficiency-stratified pancreatic ductal adenocarcinoma.* Drug Resist Updat, 2024. **76**: p. 101115.
27. Zhou, Z., et al., *Mitochondria Energy Metabolism Depression as Novel Adjuvant to Sensitize Radiotherapy and Inhibit Radiation Induced-Pulmonary Fibrosis.* Adv Sci (Weinh), 2024. **11**(26): p. e2401394.
28. Chen, Q., et al., *LACTB2 renders radioresistance by activating PINK1/Parkin-dependent mitophagy in nasopharyngeal carcinoma.* Cancer Lett, 2021. **518**: p. 127-139.
29. Lin, Y., et al., *Hyperbaric oxygen targets RCN1 to modulate ER-mitochondria crosstalk and ameliorate sorafenib resistance in hepatocellular carcinoma.* Drug Resist Updat, 2026. **85**: p. 101342.

30. Zeng, Y., et al., *Single-cell transcriptome analysis identifies MIF as a novel tumor-associated neutrophil marker for pancreatic ductal adenocarcinoma.* NPJ Precis Oncol, 2025. **9**(1): p. 293.
31. Hong, W., et al., *RECQL4 Inhibits Radiation-Induced Tumor Immune Awakening via Suppressing the cGAS-STING Pathway in Hepatocellular Carcinoma.* Adv Sci (Weinh), 2024. **11**(16): p. e2308009.
32. Okajima, D., et al., *Datopotamab Deruxtecan, a Novel TROP2-directed Antibody-drug Conjugate, Demonstrates Potent Antitumor Activity by Efficient Drug Delivery to Tumor Cells.* Mol Cancer Ther, 2021. **20**(12): p. 2329-2340.
33. Chen, Y., et al., *USP44 regulates irradiation-induced DNA double-strand break repair and suppresses tumorigenesis in nasopharyngeal carcinoma.* Nat Commun, 2022. **13**(1): p. 501.
34. Chou, J., et al., *TROP2 Expression Across Molecular Subtypes of Urothelial Carcinoma and Enfortumab Vedotin-resistant Cells.* Eur Urol Oncol, 2022. **5**(6): p. 714-718.
35. Liu, Z., et al., *TBX3 shapes an immunosuppressive microenvironment and induces immunotherapy resistance.* Theranostics, 2025. **15**(5): p. 1966-1986.
36. Shvartsur, A. and B. Bonavida, *Trop2 and its overexpression in cancers: regulation and clinical/therapeutic implications.* Genes Cancer, 2015. **6**(3-4): p. 84-105.
37. Li, S., et al., *Low-dose radiotherapy combined with dual PD-L1 and VEGFA blockade elicits antitumor response in hepatocellular carcinoma mediated by activated intratumoral CD8(+) exhausted-like T cells.* Nat Commun, 2023. **14**(1): p. 7709.
38. Xie, Y., et al., *Targeting ATM enhances radiation sensitivity of colorectal cancer by potentiating radiation-induced cell death and antitumor immunity.* J Adv Res, 2025. **74**: p. 513-530.
39. Lyu, L., et al., *Bispecific Antibody Targeting VEGF/TGF-beta Synergizes with Local Radiotherapy: Turning Tumors from Cold to Inflamed and Amplifying Abscopal Effects.* Adv Sci (Weinh), 2025. **12**(30): p. e01819.
40. Liu, Y., et al., *A protease-cleavable liposome for co-delivery of anti-PD-L1 and doxorubicin for colon cancer therapy in mice.* Nat Commun, 2025. **16**(1): p. 2854.
41. Gao, Q., et al., *Honokiol-Magnolol-Baicalin Possesses Synergistic Anticancer Potential and Enhances the Efficacy of Anti-PD-1 Immunotherapy in Colorectal Cancer by Triggering GSDME-Dependent Pyroptosis.* Adv Sci (Weinh), 2025. **12**(13): p. e2417022.
42. Zhao, K., et al., *An orally administered gene editing nanoparticle boosts chemo-immunotherapy in colorectal cancer.* Nat Nanotechnol, 2025. **20**(7): p. 935-946.

Figures

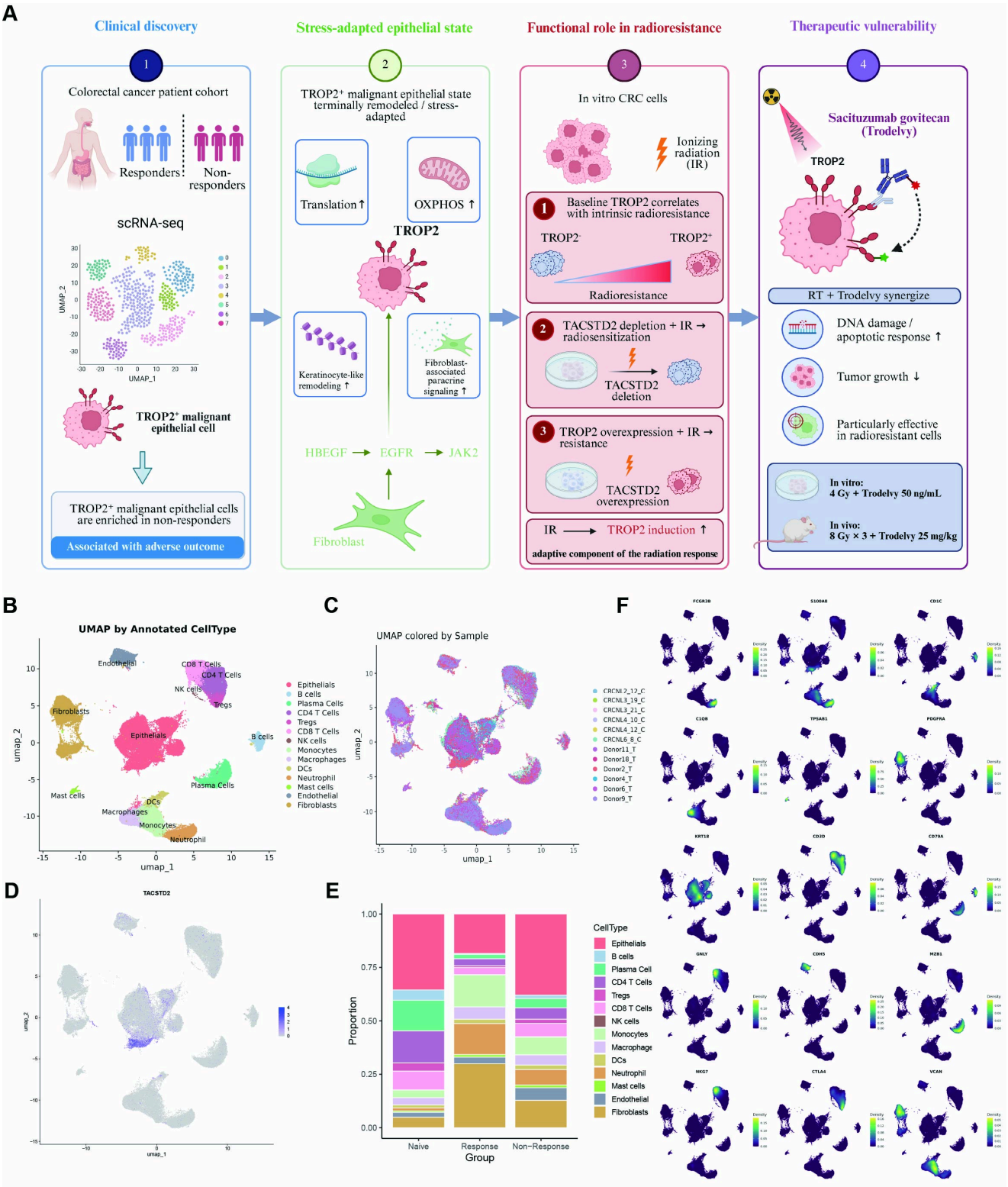


Figure 1

Single-cell transcriptomic atlas and working model of TROP2-associated radiotherapy resistance in colorectal cancer.

(A) Schematic working model summarizing the proposed role of TROP2 in CRC radiotherapy resistance and therapeutic vulnerability.

(B) UMAP visualization of the integrated single-cell transcriptomic atlas showing major annotated cell populations in colorectal cancer specimens, including epithelial cells, T cells, plasma cells, B cells, myeloid cells, endothelial cells, fibroblasts, mast cells, neutrophils, and other stromal or immune compartments.

(C) UMAP plot colored by individual sample, showing integration of cells across patient specimens.

(D) Feature plot showing TACSTD2 expression across the integrated single-cell atlas.

(E) Stacked bar plot showing the relative proportions of major cell types across Naive, Response, and Non-Response groups.

(F) Feature plots showing the expression patterns of representative lineage marker genes across the integrated UMAP.

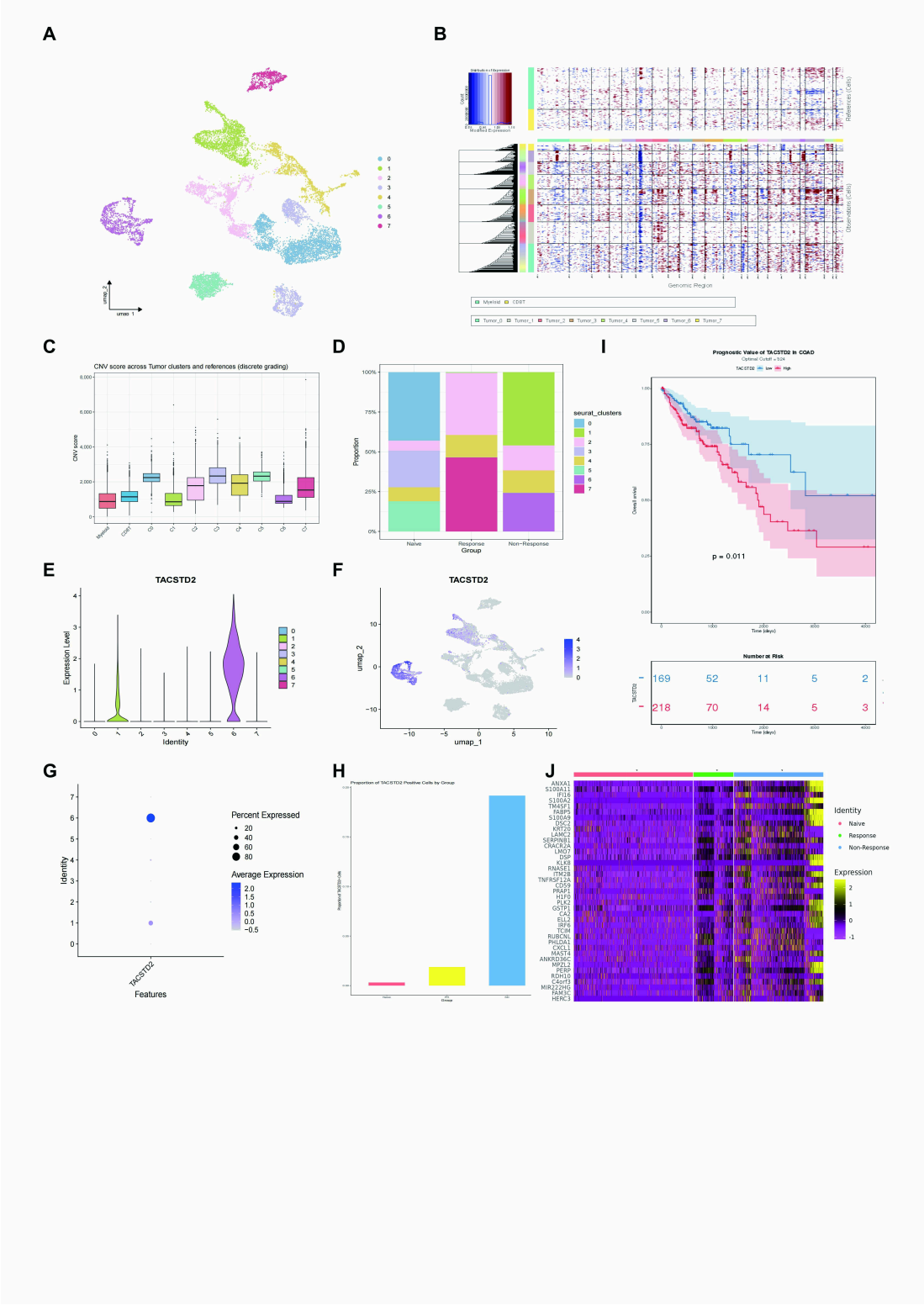


Figure 2

Identification of TROP2⁺ malignant epithelial cells enriched in radiotherapy non-responsive colorectal cancer.

(A) UMAP visualization of re-clustered epithelial cells, showing transcriptionally distinct epithelial subclusters.

(B) inferCNV heatmap showing inferred copy-number variation patterns across epithelial subclusters, with reference populations used to distinguish malignant epithelial cells from non-malignant cells.

(C) Box plot showing CNV scores across epithelial subclusters and reference cells.

(D) Stacked bar plot showing the relative abundance of epithelial subclusters across Naive, Response, and Non-Response groups.

(E) Violin plot showing TACSTD2 expression across epithelial subclusters.

(F) Feature plot showing TACSTD2 expression across the epithelial UMAP.

(G) Dot plot showing TACSTD2 expression and detection frequency across epithelial subclusters.

(H) Bar plot showing the proportion of TACSTD2/TROP2-positive malignant epithelial cells across clinical groups.

(I) Kaplan–Meier overall survival analysis of TCGA-COAD patients stratified by TACSTD2 expression.

(J) Heatmap showing differentially expressed genes associated with TROP2^{+} malignant epithelial cells across clinical groups.

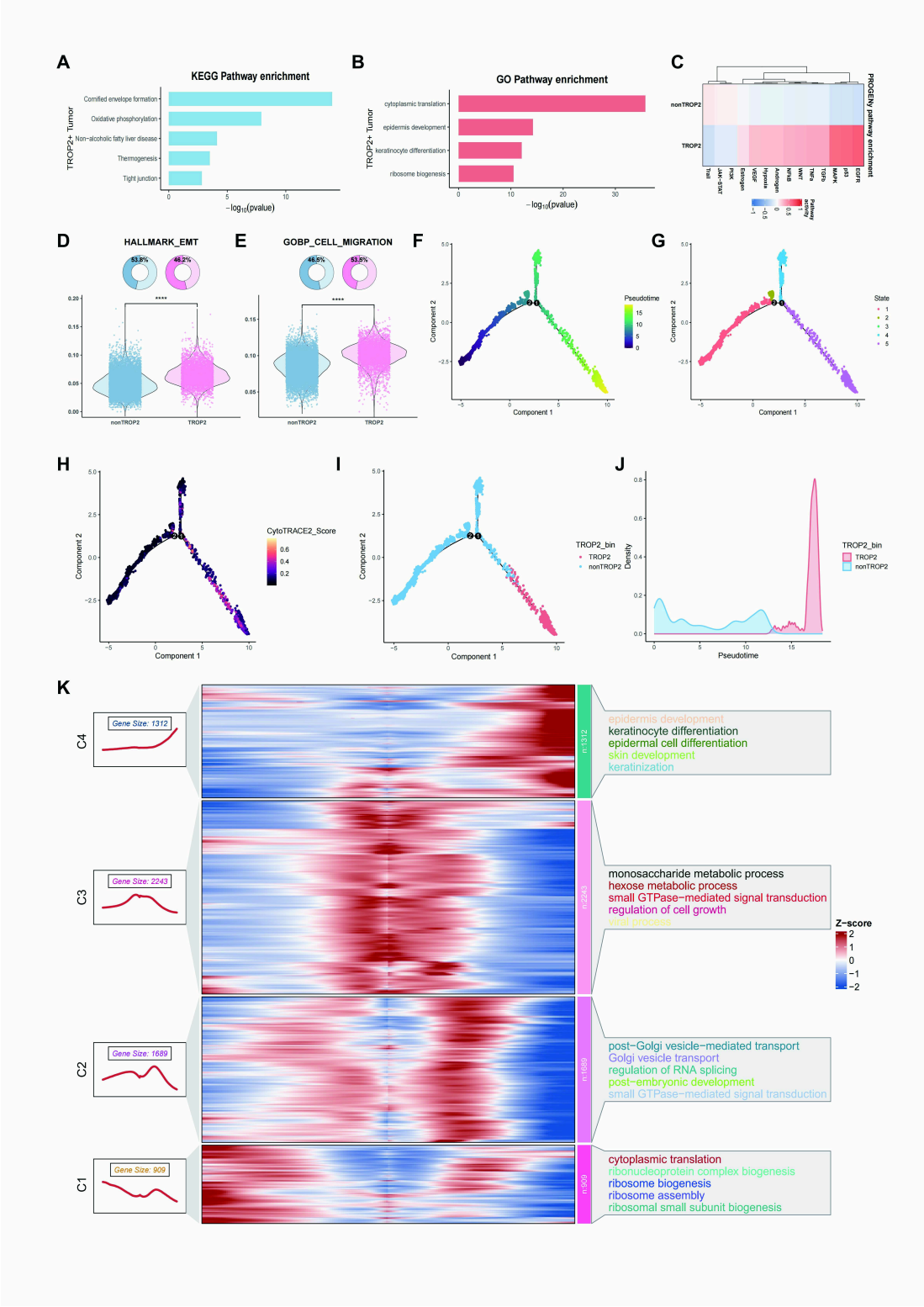


Figure 3

TROP2⁺ malignant epithelial cells occupy a terminally remodeled and stress-adapted epithelial state.

(A) KEGG pathway enrichment analysis of genes upregulated in TROP2⁺ malignant epithelial cells compared with TROP2⁻ malignant epithelial cells.

(B) Gene Ontology biological process enrichment analysis of genes upregulated in TROP2^{+} malignant epithelial cells.

(C) Heatmap showing inferred pathway activity or signaling-related transcriptional programs associated with the TROP2^{+} malignant epithelial state.

(D) UCell score comparison of the HALLMARK_EMT signature between TROP2^{+} and TROP2^{-} malignant epithelial cells.

(E) UCell score comparison of the GOBP_CELL_MIGRATION signature between TROP2^{+} and TROP2^{-} malignant epithelial cells.

(F) Monocle-based pseudotime trajectory of malignant epithelial cells colored by pseudotime.

(G) Pseudotime trajectory colored by cell state.

(H) Distribution of CytoTRACE scores along the epithelial trajectory.

(I) Mapping of TROP2^{+} and TROP2^{-} malignant epithelial cells onto the epithelial trajectory.

(J) Density plot showing the distribution of TROP2^{+} and TROP2^{-} malignant epithelial cells along pseudotime.

(K) Heatmap showing branch-dependent gene expression modules identified along the epithelial trajectory, with representative enriched biological processes annotated for each module.

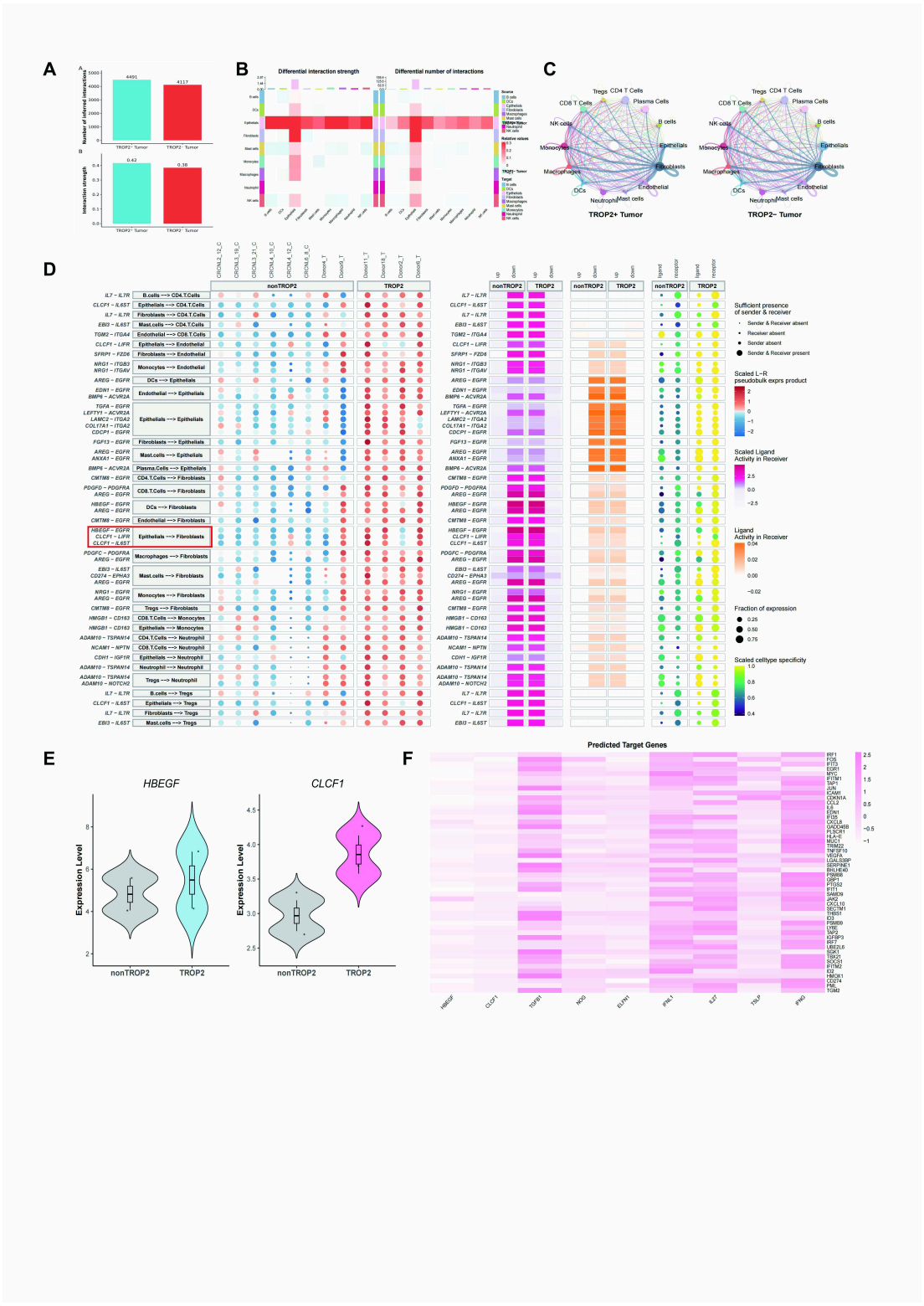


Figure 4

Cell communication analysis reveals enhanced fibroblast-associated paracrine signaling in TROP2⁺ malignant epithelial cells.

(A) Bar plots comparing the total number and overall strength of inferred cell–cell interactions between TROP2⁺ and TROP2⁻ malignant epithelial cells.

(B) Heatmap showing differential interaction strength and differential number of interactions between TROP2^{+} or TROP2^{-} malignant epithelial cells and other cell populations in the tumor microenvironment.

(C) Circle plots showing inferred communication networks between TROP2^{+} or TROP2^{-} malignant epithelial cells and major stromal, immune, and endothelial compartments.

(D) Dot plots summarizing prioritized ligand–receptor interactions, ligand activity, receptor activity, ligand expression, receptor expression, and target specificity associated with TROP2^{+} malignant epithelial cells.

(E) Violin plots showing expression levels of representative ligands, including HBEGF and CLCF1, in TROP2^{+} and TROP2^{-} malignant epithelial cells.

(F) Heatmap showing predicted downstream target genes associated with prioritized ligands.

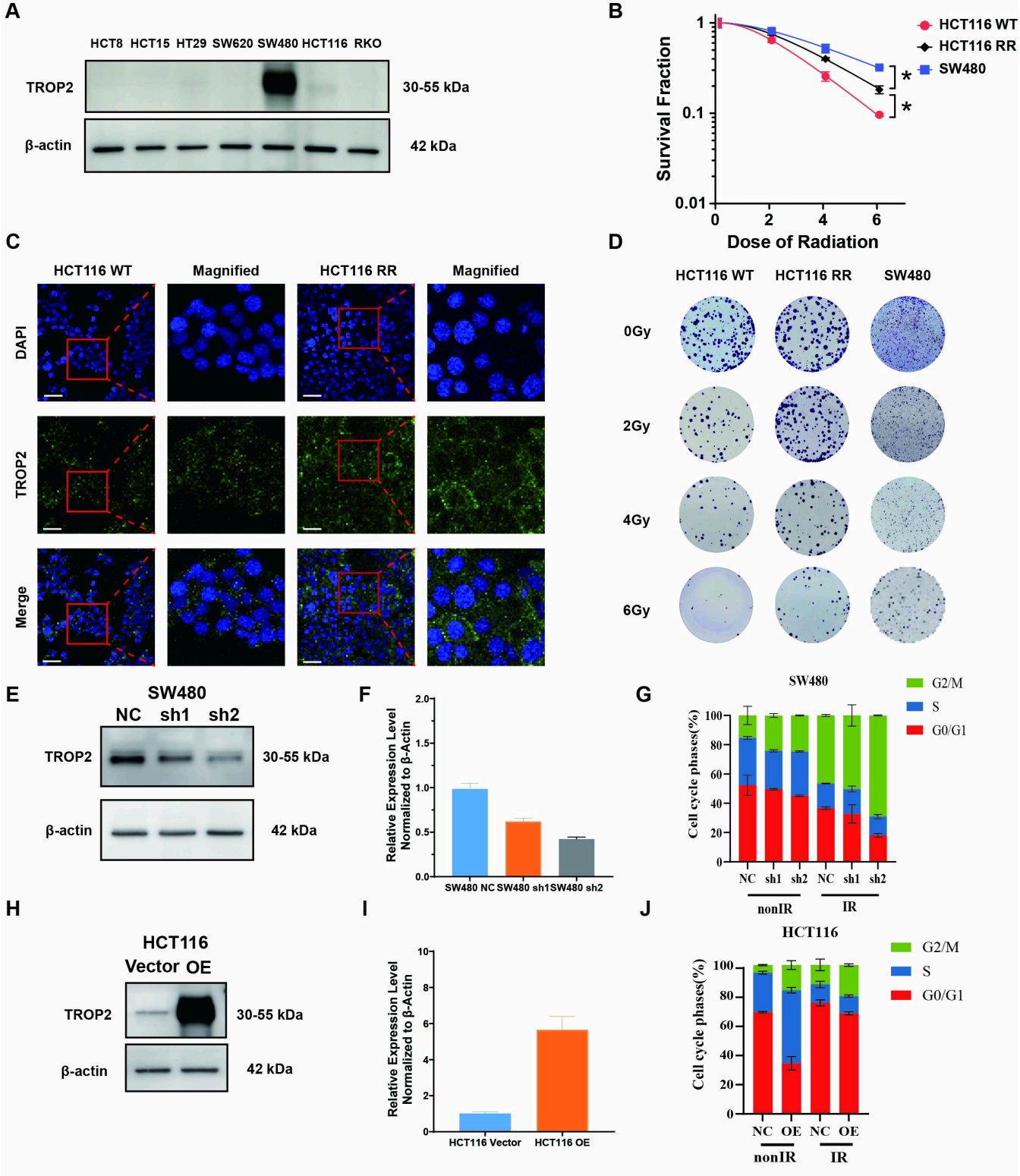


Figure 5

TROP2 expression correlates with intrinsic radioresistance and radiation-associated cell-cycle redistribution in colorectal cancer cells.

(A) Western blot analysis of basal TROP2 protein expression across a panel of colorectal cancer cell lines. β-actin was used as the loading control.

(B) Clonogenic survival curves of HCT116 WT, HCT116 RR, and SW480 cells following exposure to graded doses of ionizing radiation.

(C) Immunofluorescence staining showing TROP2 expression in HCT116 WT and HCT116 RR cells. DAPI was used for nuclear staining. Magnified regions are indicated by red boxes.

(D) Representative clonogenic formation images of HCT116 WT, HCT116 RR, and SW480 cells after exposure to 0, 2, 4, or 6 Gy irradiation.

(E) Western blot validation of TROP2 knockdown in SW480 cells expressing control shRNA or two independent TACSTD2-targeting shRNAs.

(F) Quantification of TROP2 protein expression in SW480 control and knockdown cells, normalized to β-actin.

(G) Flow-cytometric analysis of cell-cycle distribution in SW480 control and TACSTD2-knockdown cells under non-irradiated and irradiated conditions.

(H) Western blot validation of TROP2 overexpression in HCT116 cells.

(I) Quantification of TROP2 protein expression in HCT116 vector-control and TROP2-overexpressing cells, normalized to β-actin.

(J) Flow-cytometric analysis of cell-cycle distribution in HCT116 control and TROP2-overexpressing cells under non-irradiated and irradiated conditions.

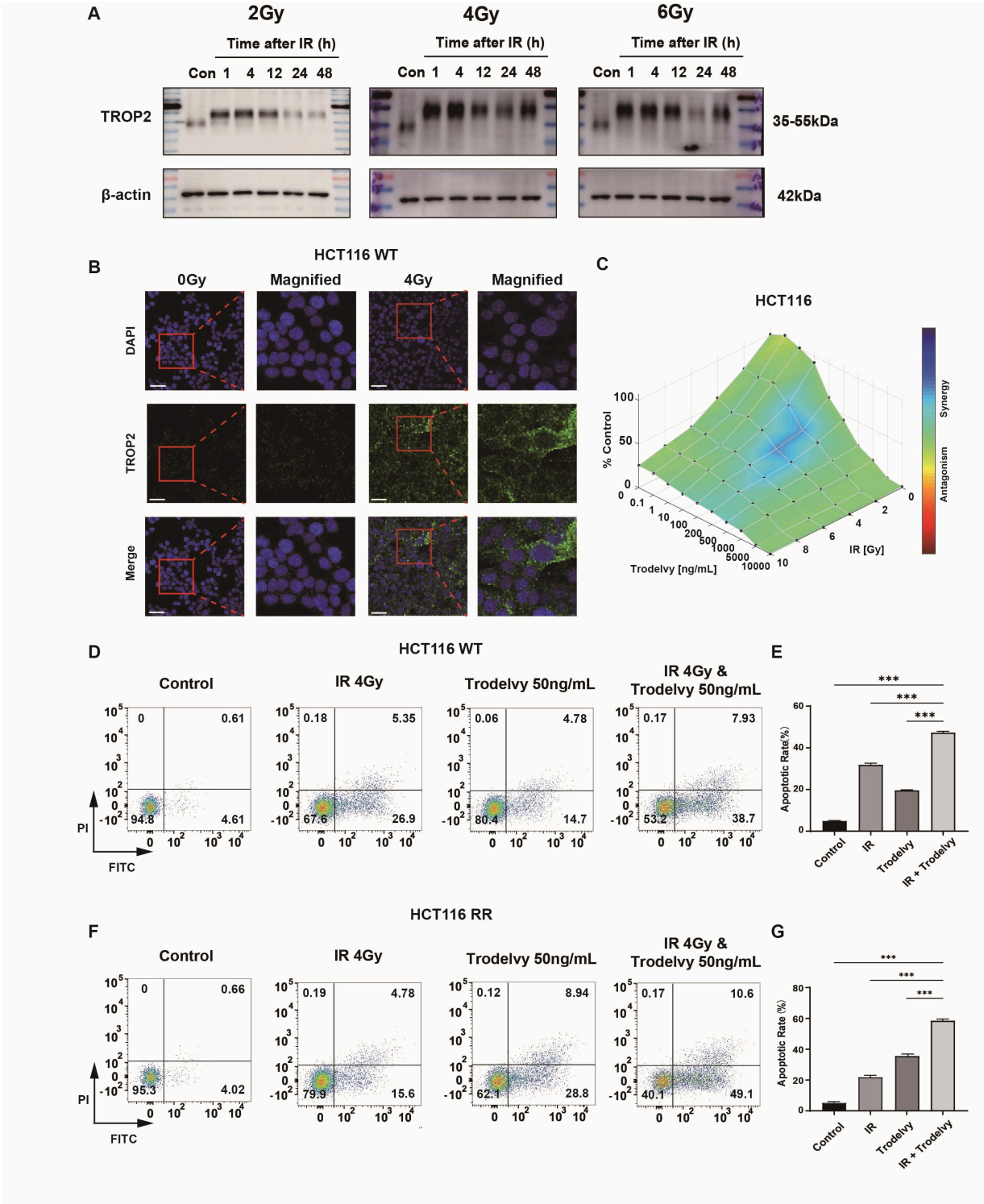


Figure 6

Radiation-induced TROP2 expression creates a therapeutic vulnerability to Trodelvy.

(A) Western blot analysis showing dynamic changes in TROP2 protein expression in HCT116 cells at indicated time points after exposure to 2, 4, or 6 Gy ionizing radiation. β-actin was used as the loading control.

(B) Immunofluorescence staining showing TROP2 expression in HCT116 WT cells under non-irradiated conditions and after 4 Gy irradiation. DAPI was used for nuclear staining. Magnified regions are shown.

(C) Response-surface analysis showing the combined effect of graded irradiation and increasing concentrations of sacituzumab govitecan (Trodelvy) on HCT116 cell viability. The response surface illustrates the interaction between irradiation dose and Trodelvy concentration.

(D) Representative Annexin V-FITC/PI flow-cytometry plots of apoptosis in HCT116 WT cells treated with control, 4 Gy irradiation, Trodelvy, or the combination of irradiation and Trodelvy.

(E) Quantification of apoptotic rates in HCT116 WT cells under the indicated treatment conditions.

(F) Representative Annexin V-FITC/PI flow-cytometry plots of apoptosis in HCT116 RR cells treated with control, 4 Gy irradiation, Trodelvy, or the combination treatment.

(G) Quantification of apoptotic rates in HCT116 RR cells under the indicated treatment conditions.

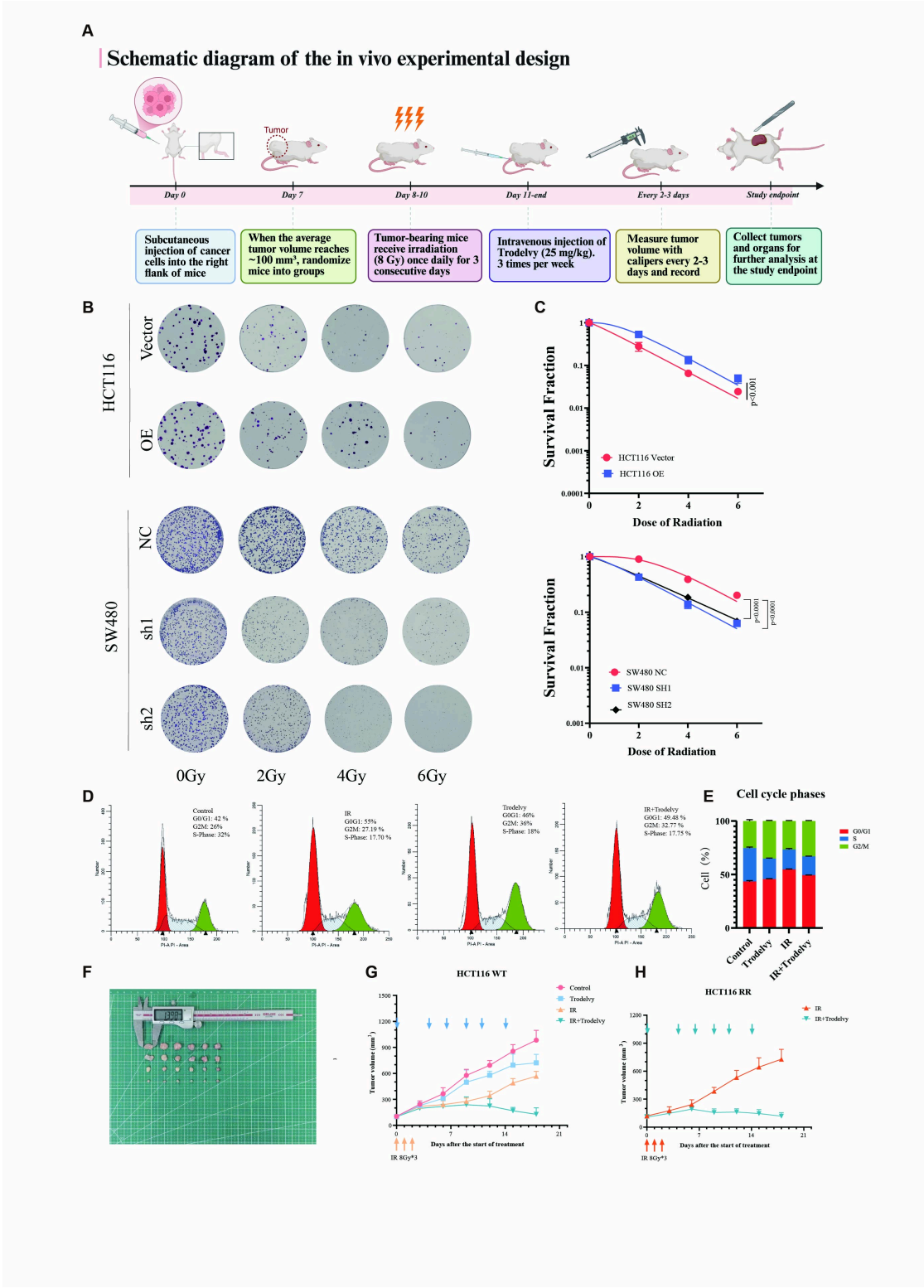


Figure 7

Genetic and pharmacological targeting of the TROP2 axis enhances radiosensitivity and improves in vivo tumor control.

(A) Schematic diagram of the in vivo experimental design. Tumor cells were subcutaneously implanted into mice. When tumors reached approximately 100 mm³, mice were randomized into treatment groups

and treated with local irradiation, Trodelvy, or the combination. Tumor volume was measured every 2–3 days until the study endpoint.

(B) Representative clonogenic formation images of HCT116 vector-control and TROP2-overexpressing cells, as well as SW480 control and TACSTD2-knockdown cells, following exposure to 0, 2, 4, or 6 Gy irradiation.

(C) Clonogenic survival curves showing the effects of TROP2 overexpression in HCT116 cells and TACSTD2 knockdown in SW480 cells on radiosensitivity.

(D) Representative propidium iodide DNA-content histograms showing cell-cycle distribution in CRC cells treated with control, Trodelvy, irradiation, or irradiation plus Trodelvy. The proportions of cells in G0/G1, S, and G2/M phases are indicated.

(E) Quantitative stacked bar plot showing the proportions of cells in G0/G1, S, and G2/M phases under the indicated treatment conditions.

(F) Representative images of excised xenograft tumors collected at the study endpoint after the indicated treatments.

(G) Tumor growth curves of HCT116 WT xenografts treated with control, Trodelvy, irradiation, or irradiation plus Trodelvy.

(H) Tumor growth curves of HCT116 RR xenografts treated with irradiation alone or irradiation plus Trodelvy.

Supplementary Files

This is a list of supplementary files associated with this preprint. Click to download.

- SupplementaryMaterials.docx